Digital Terrain Analysis of Sea-land Combined Data on the Outer Zone of Southwest Japan Including the Nankai Trough

Junko IWAHASHI[1], Yuki MATSUSHI and Hiroshi FUKUOKA[2]

(1) Geospatial Information Authority of Japan.

(2) Niigata University

Synopsis

We analyzed drainage networks, profiles, and terrain types of Southwest Japan using a 490-m DEM and a 150-m DEM, both of which were mosaics of land elevation by the Geospatial Information Authority of Japan and seafloor elevation by the Japan Coast Guard. Moreover, we visualized land topography and other data, i. e., seismic tomography data, distribution of seismic intensity, and plate boundary data that were published on the Internet. The visualization shows inhomogeneous structure of velocity below the Japanese islands and a clear hot section leading out from deep underground to Osaka Bay. Land and shelf edges are quantitatively similar to each other in topography. However, there are almost no steep slopes with high valley density on the seafloor in contrast to land surfaces. Instead of high valley density slopes, long large steep slopes as in Holocene volcanos, such as Mt. Fuji, are widely distributed on the deeper seafloor. In addition, steeper parts of long large slopes are distributed around active faults in land, inner trench areas and outer ridges on the seafloor, in addition to tops of volcanos.

Keywords: terrain classification, topography, drainage network, Nankai Trough, seismic tomography, Southwest Japan

1.   Introduction

Geomorphological studies have been done in predominantly land areas, and usually have been treated separately: divided into either land or seafloor, even for continuous situations such as volcanic islands. Except for some advanced efforts such as in the field of active faults (Tsutsumi et al., 1990), most geomorphological studies focus only on land. However, many parts of the Japanese archipelago in Southwest Japan were formed by lifting of the seafloor associated with plate sinking in trenches. The Outer Zone of Southwest Japan, which is the object of this study, was formed by phenomenon which occurred under the sea.

We considered that we should visualize and analyze sea-land combined data, in addition, we should observe the data more three-dimensionally. Therefore, we examined the three issues below:

1) Drainage network and watersheds – from land to the Nankai Trough
2) Classification of the sea-land topography
3) Cross-sections of the 3-D images of underground structures with a sea-land shaded-relief image

2.   Mosaic of the elevation data

The most widely used nationwide DEM (Digital Elevation Model) in Japan is the 10-m DEM of the

Table 1 Specifications of DEMs used in this study.

	1) The 10-m DEM in the Base Map Information	2) J-EGG 500	3) Geographical Feature Meshes Data (3rd and 4th mesh)	Combined DEMs in this study
Publisher	GSI	JCG and JAMSTEC	JCG	-
Covered area	Land (Japan)	Sea (Japan and its surroundings)	Sea (coastal area only)	490-m: E 150-141°, N 30-38° 150-m: land and coastal area
Unit of elevation	10-cm	1-m	1-m	1-m
Standard of grid	Geographic (lat-long)	Lambert conformal conic	Lambert conformal conic	Lambert conformal conic
Grid size	0.4" (11-12m in Lambert conformal conic)	Approximately 500-m	4th mesh: approximately 150-m, 3rd mesh: approximately 450-m	490-m or 150-m
Geodetic reference system	JGD2000	WGS84	WGS84	WGS84
Data source	Contours in 1:25,000 topographic maps of GSI	Single and multi-beam sounding depth, Contours in 1:1,000,000 map of JCG	J-EGG 500, J-BIRD, and other sounding depth	490-m: 1), 2) and 3rd mesh of 3) 150-m: 1) and 4th mesh of 3)
Accuracy of heights	±2.5-5m	unknown	unknown	-

Base Map Information (Table-1) prepared by the Geospatial Information Authority (GSI). In this study, we used reduced data of the 10-m DEM. The original data of the 10-m DEM are contour lines which were figured in 1:25,000 scaled topographic maps of GSI. Therefore the 10-m DEM came from one kind of source and includes homogeneous accuracy.

In the case of marine topography, the Japan Coast Guard (JCG) has been preparing some data. We used 3rd mesh and 4th mesh of Geographical Feature Meshes Data of JCG, and J-EGG 500 (JODC-Expert Grid data for Geography) of JCG and the Japan Agency for Marine-earth Science and Technology (JAMSTEC) (Table 1). Marine topographic maps originally have their own standard of height which is different from that in land topographic maps. However, the data in Table 1 include elevation data which had been converted to the same standard of land data, which is Tokyo Bay's mean sea level. The main characteristic of the seafloor DEM is that it is not a single source like the land DEM. As the state of true data and interpolation data which can be observed from the code number of J-EGG 500 suggests, seafloor DEM is made by a great variety of sources, both survey methods and survey timing, such as contour lines and elevation data along with punctate trails of ultrasonic survey (Asada, 2000).

Table 1 also shows the combination method of sea and land DEMs. We gave priority to the land data which has better accuracy for overlapped areas. The standard of the combined DEMs were adjusted to the seafloor DEM, for avoiding re-interpolation

of coarse seafloor DEM. Fig. 1 shows a bird-eye-view image of the combined data.
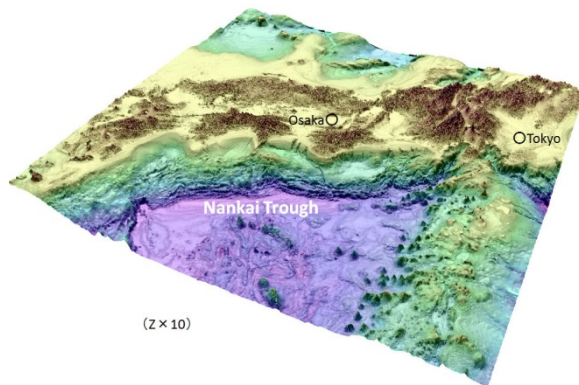

Fig. 1 Bird-eye-view image of the combined data.

3. Drainage network and watershed – from land to the Nankai Trough

In land areas, hydrological geography has been studied and a method to extract drainage networks and their watersheds from a DEM has been developed (Tarboton, 1997; Maidment, 2002). Fig. 2 shows drainage patterns (black lines) which were thresholded from flow accumulation data of the 490-m DEM by the value almost coinciding with the first-class rivers designated by the Ministry of Land, Infrastructure, Transport and Tourism (MLIT); and their watersheds (black lines).

Downstream meandering on gentle slopes was shortened in the drainage networks calculated from the 490-m DEM. The places where drainage lines gather coincide with the post-Pleistocene turbidite deposits (yellow in Fig. 2) on the marine geological map (Okuda, 1977). From the 490-m DEM, watersheds which continue to the Nankai Trough are few and we could not find watersheds which fall to the Kumano ocean basin or the Hyuga ocean basin.

Fig. 3 shows profiles of five large rivers (Fuji, Tenryu, Hidaka, Niyodo, and Shimanto River) along with the drainage lines. The watersheds of these five rivers continue to the Nankai Trough. In case of the Fuji River and the Tenryu River, continental slopes begin at zero elevation shores. However, in case of the other three rivers which lie in western Kinki, the shelf continues to 140-m depth from the land slopes. A profile created from a coarse DEM such as the 490-m DEM tends to be a straight line in eroded areas, therefore not only the land areas but the continental shelf cut by the Hidaka River shows a linear profile. Each profile in Fig. 3 has its own characteristics, however, the Niyodo River and Shimanto River, which travel to the same ocean basin, the Tosa ocean basin, show similar profiles.
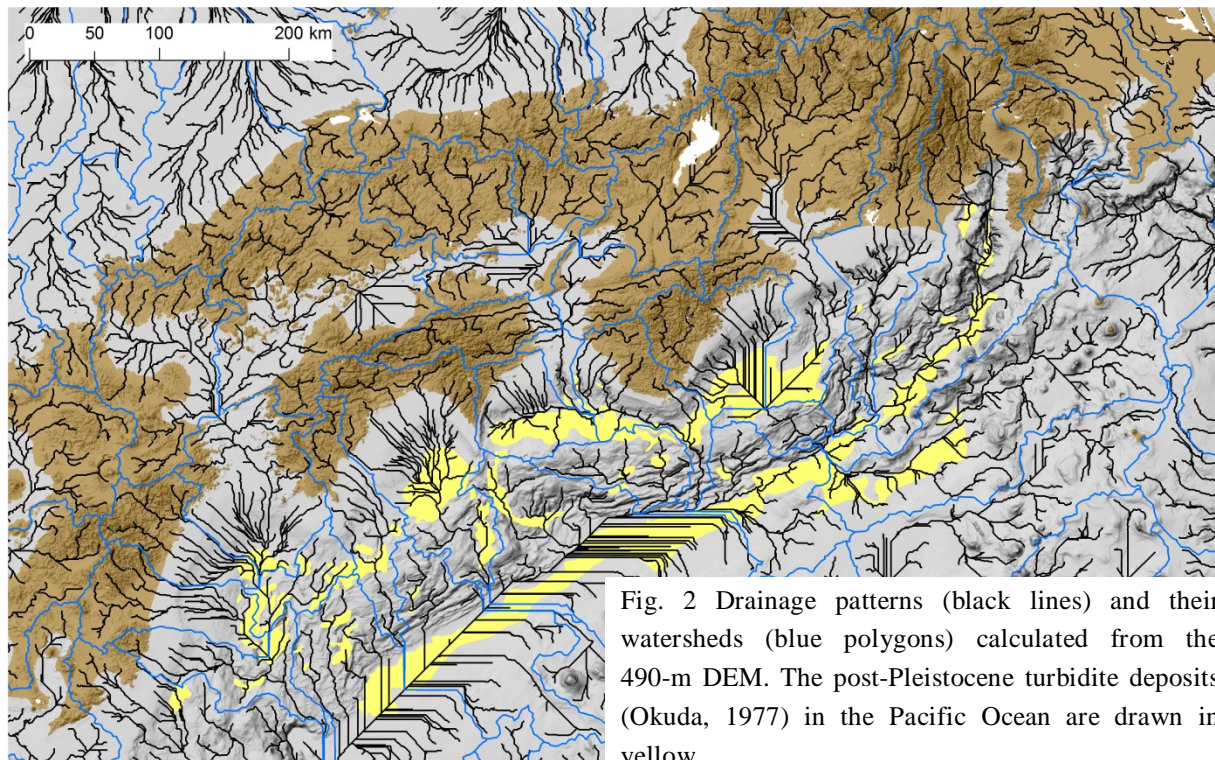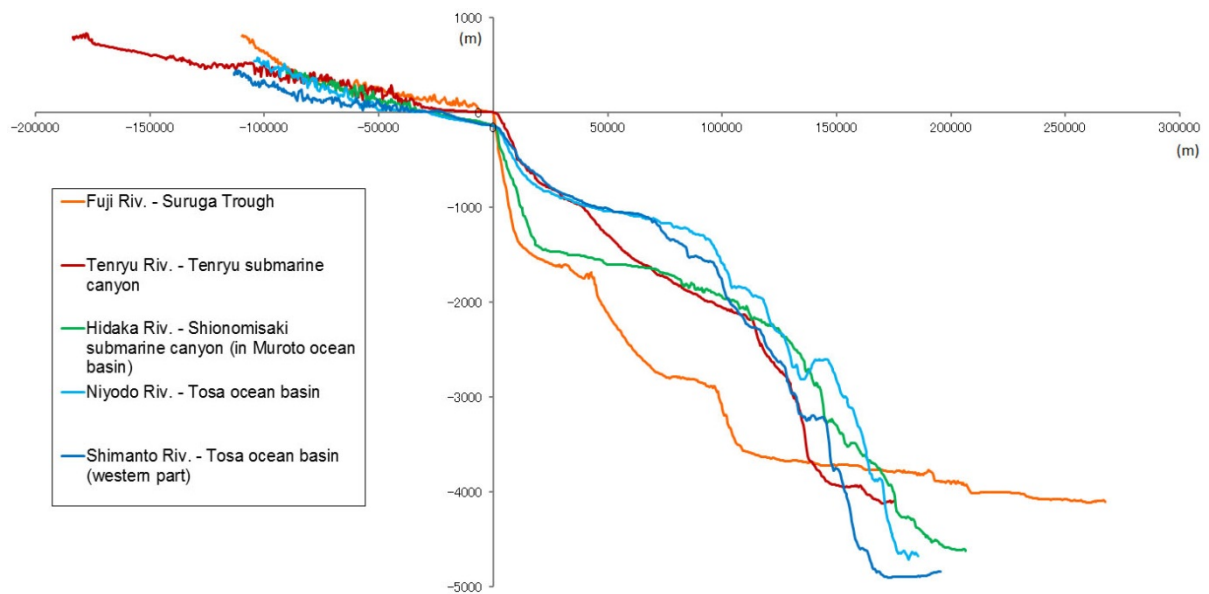

Fig. 2 Drainage patterns (black lines) and their watersheds (blue polygons) calculated from the 490-m DEM. The post-Pleistocene turbidite deposits (Okuda, 1977) in the Pacific Ocean are drawn in yellow.

Fig. 3 Profiles of the five rivers calculated from the 490-m DEM along with drainage lines, from the land to the Nankai Trough.

4. Classification of the sea-land topography

The corresponding author studied in the DPRI of Kyoto University as a former in-country exchange student and developed a method of pixel-based automated classification of topography using DEMs by image processing techniques (Iwahashi, 1994; Iwahashi and Kamkiya, 1995). Subsequently, the corresponding author arranged the method to fit GIS software such as ArcGIS (ESRI) and produced 1-km grid worldwide terrain classification data using SRTM-30 (Iwahashi and Pike, 2007). This data and method has been used for studies of seismic damage or response by topographic amplification (Hough et al., 2010; Yong et al., 2012), soil condition (Reuter et al., 2008), marine topography (Gorvini, 2009) and so on.

The former method (Iwahashi and Pike, 2007) use the three geometric signatures calculated from a DEM. At first, the slope gradient was introduced as a fundamental parameter for dividing mountains and other areas. The surface texture, which is a focal density of pits and peaks extracted by median filter from a DEM, tend to have low values in Holocene volcanos or alluvial fans. The local convexity, which is a focal density of convex points extracted by the Laplacian filter from a DEM, tends to have high values in terraces. These three geometric signatures can be calculated not only in 3-by-3 cells, but also in expanded larger window sizes (Iwahashi et al., 2009). The method of classification is very simple. Combination of the three binary data which are created by binarization using mean values of the three signatures can create classified data (Fig. 4). Gentler slopes can be re-classified using its mean values, i.e., exponentially set threshold values (nested-means algorithm). The result can be summarized as Series I to IV (Fig. 4).

The former pixel-based method will enable to create satisfactory classification maps when using hundreds of meters grid DEMs. However, there are some problems in the pixel-based method. At first, it is difficult to handle scale issues and noises in high-resolution DEMs; second, pixel data is hard to join with thematic data; and there is a large volume of data. Therefore, the new method has been developed.

In recent years, object-based image segmentation techniques have been developing and many examples of usage can be found in the remote sensing field, such as forest classification or building detection (Hay et al., 2005; Blaschke, 2010). Baatz and Schäpe (2000) developed a multiresolution segmentation technique and we can use it in the eCognition (Trimble). The multiresolution segmentation technique calculates
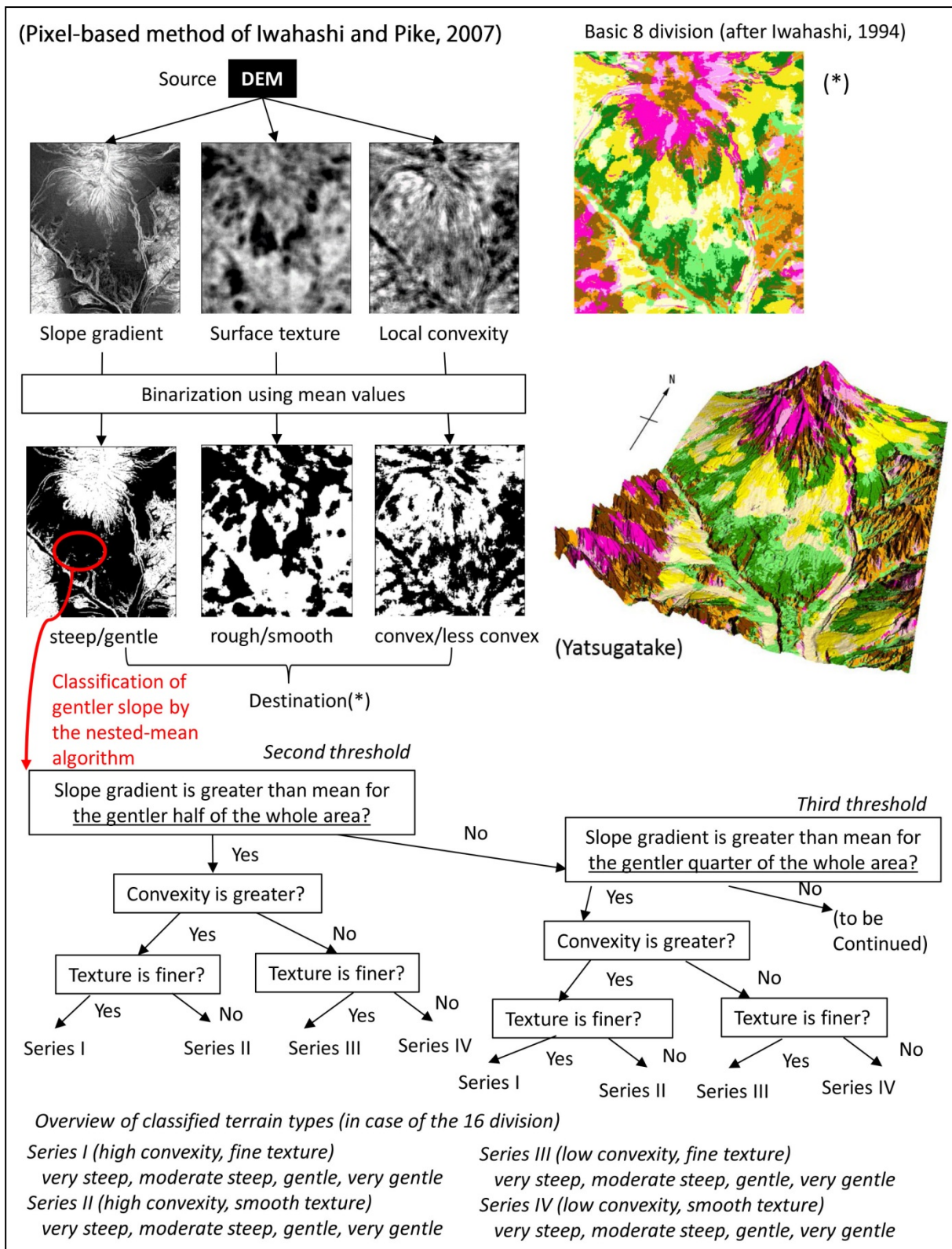
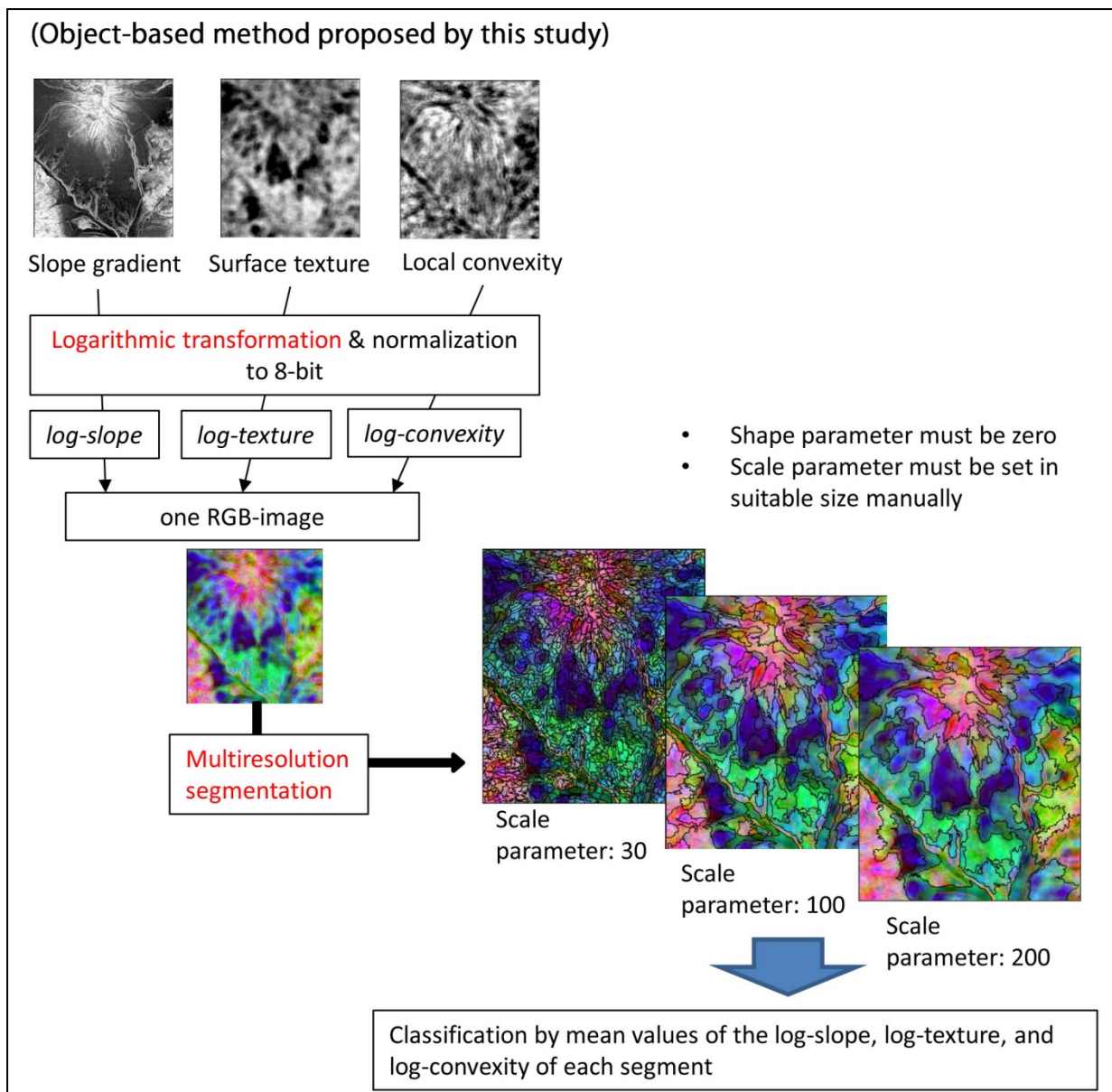Fig. 4 Pixel-based terrain classification using DEM by Iwahashi and Pike (2007).

Fig. 5 Object-based terrain classification using DEM proposed by this study.

similarity of adjacent image objects (*Degree of Fitting*) and merges pixels which have more similarity than the least value (the scale parameter), then make one larger object and return it as a polygon. The number of the geometric signatures used in the former method was three. After normalization to 8-bit (after this, we call normalized logarithmic values of the three geometric signatures the log-slope, log-texture, and log-convexity), they can be composed to one RGB image and must be classified.

The revised method is described in Fig. 5. The geometric signatures are the same with those of the former method. The reason for transforming them

to logarithmic values before normalization is to correspond with the nested-means algorithm. Polygon sizes of a destination data can be changed by the scale parameter. We set the suitable scale parameters manually, and set it as 30 for the 490-m and 150-m DEMs. For the other parameters in eCognition, the shape parameter was set to zero, and the compactness was set to 0.5.

The most difficult point of the object-based classification lies after image segmentation. The point is how to make groups by statistical values of the log-slope, log-texture, and log-convexity in each polygon. We used mean values of the three variables calculated in each polygon. The first

solution is the simple thresholding: to use the mean values of the whole area or the values at regular intervals. Grouping can be done by multi-slice classification. This grouping method is essentially equivalent to the classification technique of Iwahashi and Pike (2007). Strengths of this technique are that it is easy, but the destination may be a fairly good result, and that it is available for an area without training data. Weaknesses are that it has a possibility of large differences compared to existing thematic maps, and the threshold values would not be applicable to other regions. The second solution is an automatic classification, clustering (MacQueen, 1967). Strengths of clustering are the possibility of automated classification, numerical validity, and saving time and labor. One weakness is that the clustering would not be applicable to other regions. The last solution also uses a multi-slice technique, but threshold values are set manually from a well-known area. To set threshold values, the scatter diagrams of the expected terrain class estimated from former research results and the three values (log-slope, log-texture, log-convexity) must be compared. Strengths are that we know why we use these threshold values; threshold values can be applicable to other unknown regions; and if the DEM includes various levels of data accuracy, this method may be the best. Weaknesses are that this method needs many materials to be compared (air-photo interpretation map, geological map, etc.) and needs much time and labor. Moreover, it may be difficult to find suitable threshold values for a high resolution DEM which includes noise such as artificially transformed land.

Topography is formed by composition of material and process. At first, we investigated the relationship between diagenesis/erosion and the three geometric signatures. Fig. 6 shows the zonal average values of the log-slope, log-texture and log-convexity calculated from the 150-m DEM for each age of sedimentary rocks (Geological Survey of Japan, 2014). The relation with original three geometric signatures can be observed as log-log scales. The slope gradient constantly increases till Miocene. The surface texture and the local convexity reach their ceiling earlier. Those inflection points may be candidates for the

threshold values. In addition, it is clear that regression analysis will not work, because the relation between diagenesis/erosion and the three geometric signatures are not simple even in sedimentary rocks.
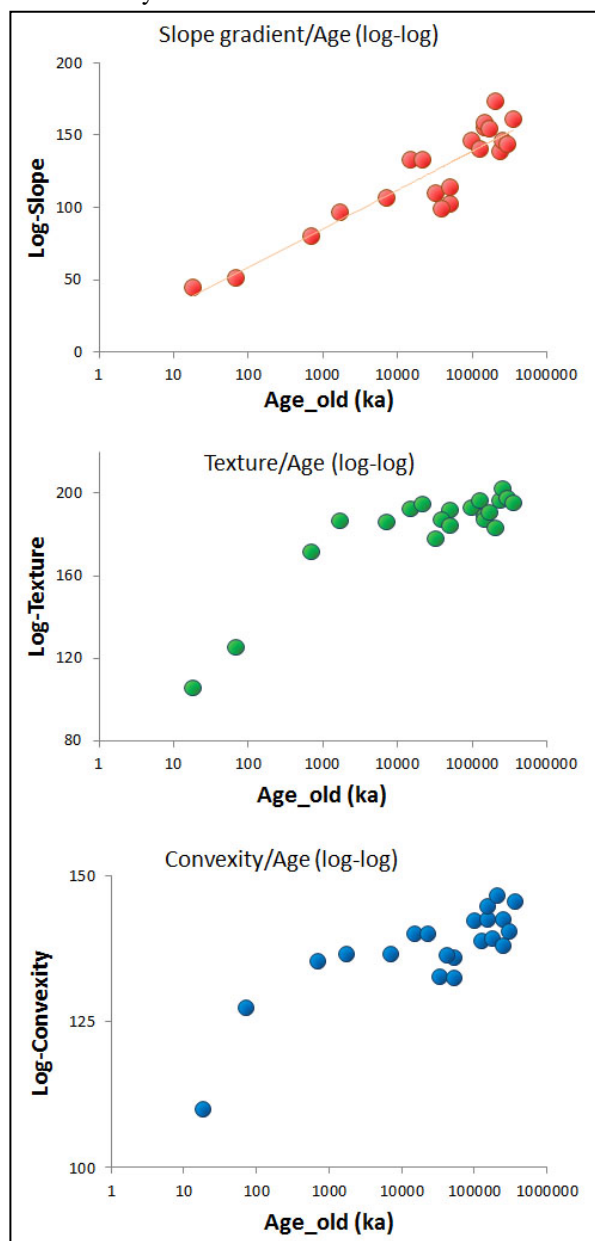

Fig. 6 Zonal average values of three geometric signatures calculated from the 150-m DEM for each age of sedimentary rocks.

Fig. 7 shows the zonal average values of the log-slope and log-convexity compared with the legends of the 1:25,000 Land Condition Maps of GSI. With regard to terraces, though individual mean values of segmented polygons are varied, in total they tend to have high convexity with erosion rate.
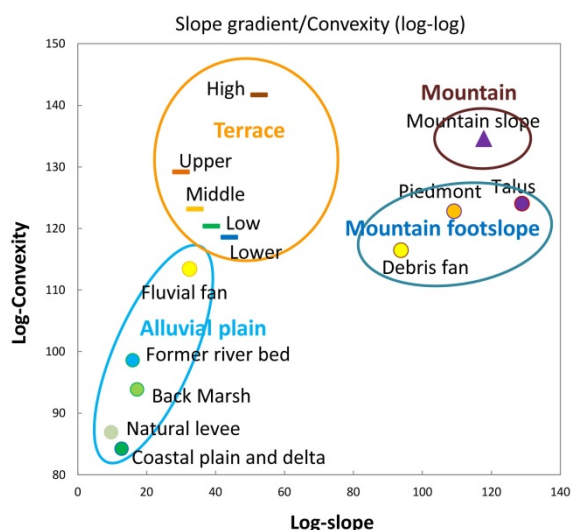
Fig. 7 Zonal average values of the log-slope and log-convexity calculated from the 150-m DEM for each terrain type described in the 1:25,000 Land Condition Map of GSI.

Fig. 8 shows scatter diagrams of the mean values of the log-slope and log-texture for the selected polygon attributes from segmented RGB images using the 150-m DEM. Terrain types were sourced from documents of nationwide terrain classification (Japan Association for Quaternary Research, 1987; Kaizuka et al., 2000; Machida et al., 2001; Ota et al., 2004; Machida, 2006; Land Condition Maps of GSI). The Landslide Distribution Map (NIED) was used to calculate the percentage of landslide masses. In the case of sedimentary rocks, it is clear that alluvial plains, terraces, hills and mountains can be divided by the slope gradient (Fig. 8-a). In gentler slopes, the surface texture increases with the slope gradient, however, it reaches the limit around the values of hills. This alteration may coincide with occurrences of landslides. From Fig. 8-b, we can find that terraces and fans are clearly divided and Holocene volcanos also have clear numerical characteristics. However, it is quite difficult to find suitable threshold values to divide more varied kinds of mountain slopes which were formed by various processes and components (Fig. 8-b). We recommend to make a classification by clustering at first, then go back to the original mean values of the three signatures and find threshold values, then make a multi-slice classification.
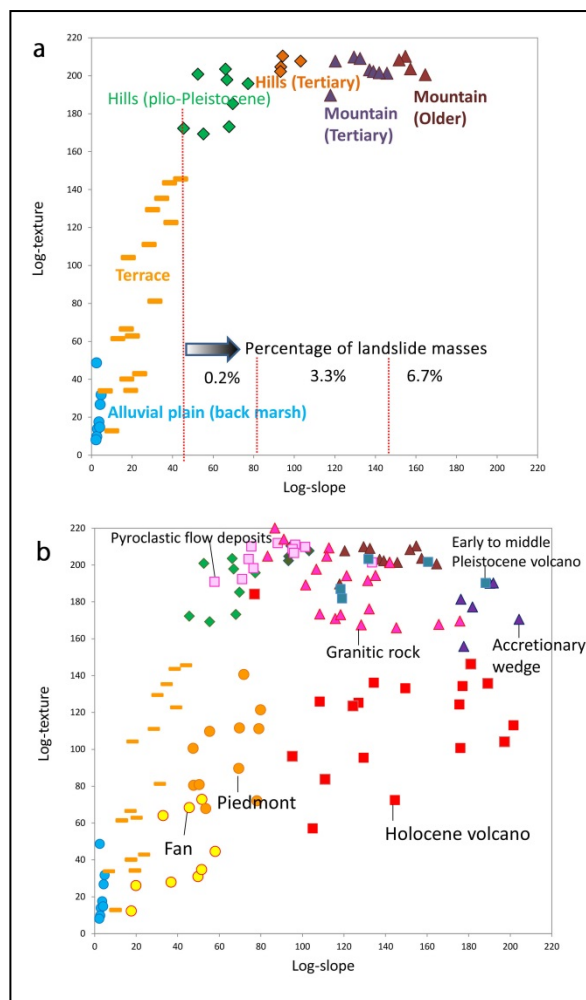

Fig. 8 Scatter diagrams of the log-slope and log-texture of some selection of polygon attributes (mean values in a polygon) calculated from segmented RGB image using the 150-m DEM: (a) sedimentary rocks and sediments, (b) various types of rocks and sediments were added.

Seafloor DEMs include various sources and various densities of elevation points. Fig. 9 shows the density of real data (not interpolated) in the 490-m DEM. Fig. 10 shows the examination of the slope gradient and the surface texture calculated by reduced DEMs, which used sample data made from a part of the seafloor data (black polygon in Fig. 9). The slope gradient and the surface texture increase logarithmically with increase of DEM grid size. The log-convexity can be ignored, because it is free from data resolution in principle. We could make rough corrections of data using the approximate curves of Fig. 10 as estimated correction curves. However, places which vary remarkably in data accuracy may not be corrected by estimated

correction curves only. We settled such a case as in Fig. 11. We corrected the threshold values which were found on the land, not the pixel values themselves. At first, we collected the values of the log-slope and the log-texture which are estimated to be neighboring pairs in the same topographic units. Then we obtained correction curves from the scatter diagrams (Fig. 11). The result may not be perfect, but it shows enough continuity.
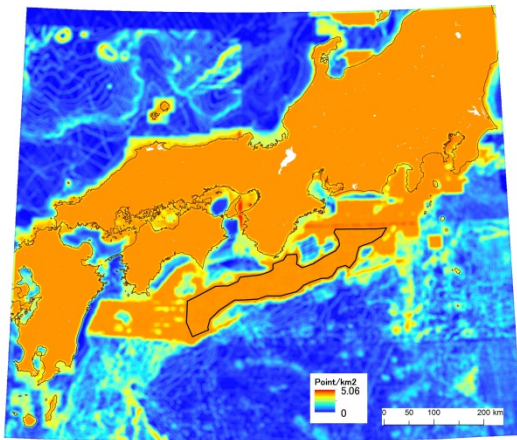

Fig. 9 The density of real data (not interpolated) in the 490-m DEM. A Black polygon in the seafloor shows the area used in Fig. 10.
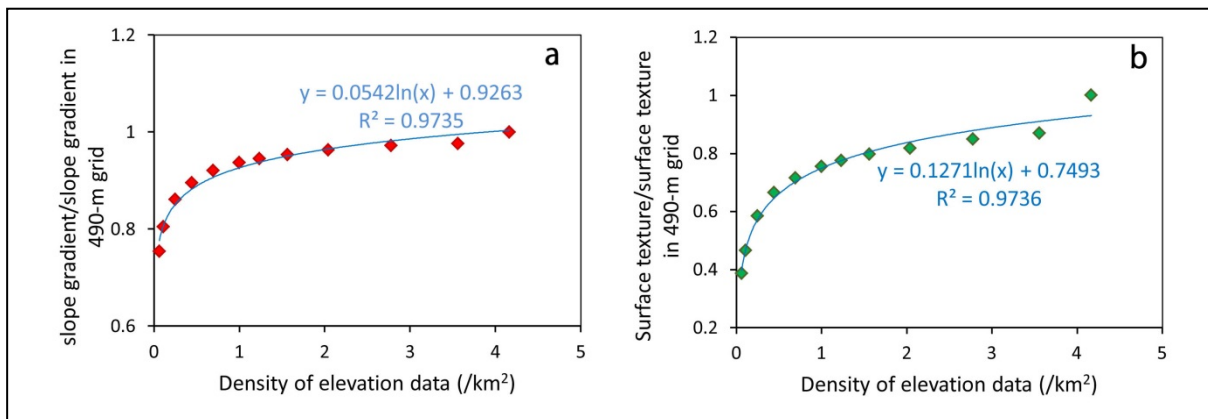

Fig. 10 Ratio of the slope gradient (a) and the surface texture (b) calculated by reduced DEM and the 490-m DEM.
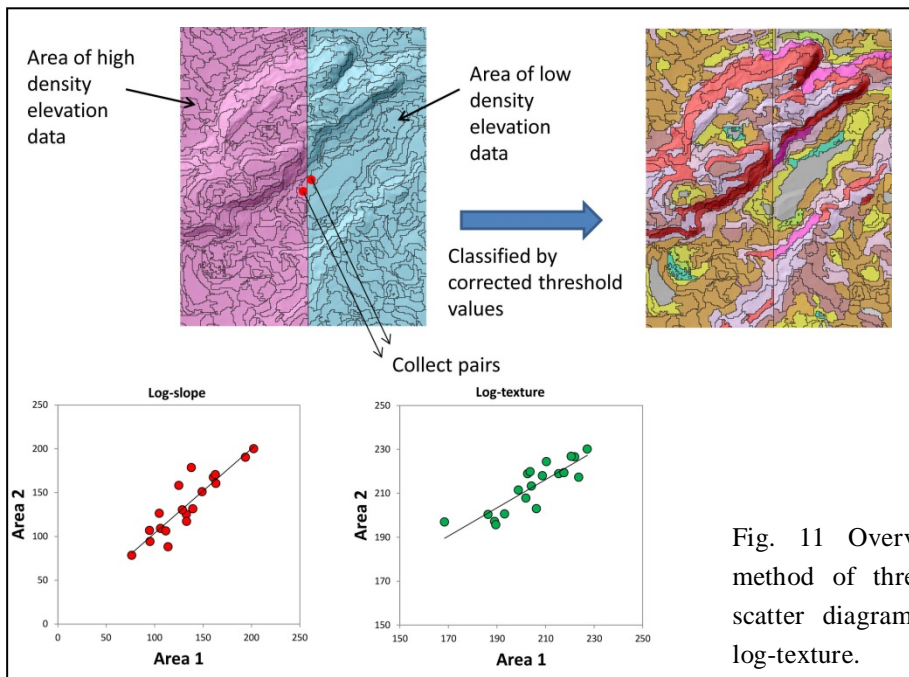

Fig. 11 Overview of the correction method of threshold values using the scatter diagrams of the log-slope and log-texture.
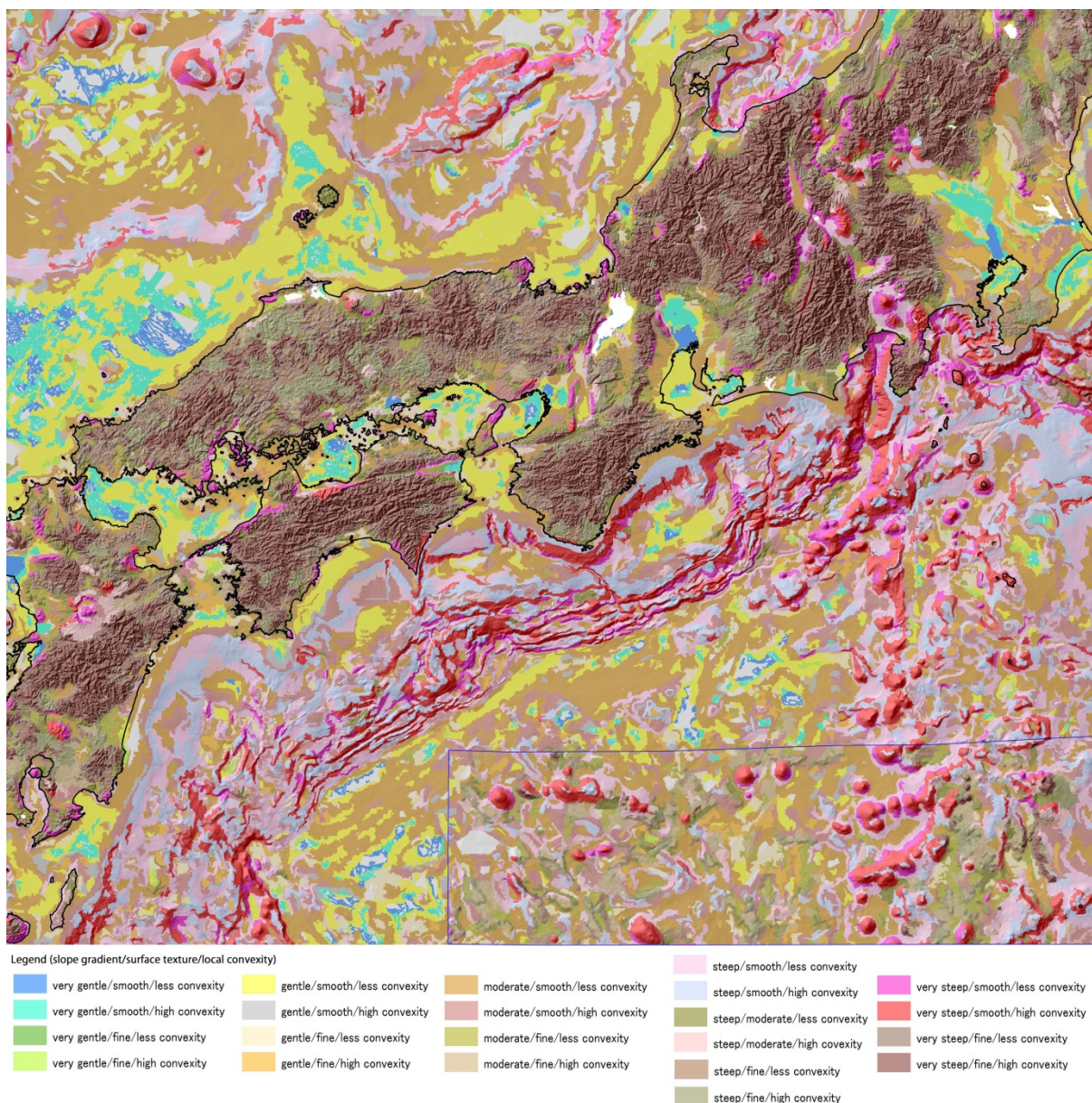
Fig. 12 Terrain classification using the 490-m DEM. This map was created by object-based image segmentation using the three geometric signatures and multi-sliced classification. The areas where the density of original elevation data is coarser than 0.0625 point/km^2 were omitted. The area inside the blue square includes obvious noises in the original DEM. A high-resolution image can be found in Appendix-1.

Fig. 12 shows multi-sliced classification using manual set threshold values from the image segmented polygons of the 490-m DEM. A high resolution version can be found in Appendix-1. On land, the very steep and smooth slopes (shown in pink or red in Fig. 12) are distributed in small and special areas, such as Holocene volcanos or slopes along with active faults. However, those types of slopes can be widely found on the seafloor. They are distributed in marine volcanos, faults on accretionary prisms, and the continental shelves where collapses occur. The very steep and fine slopes (blown in Fig. 12), which are the main objects on the land mountains, are rarely found on the seafloor. Almost all of the steep slopes on the seafloor are smooth types. Some doubts still remain, if the seafloor slopes truly lack fine texture slopes or not, because of the difference in survey method compared with the land; however, basically we considered this as follows. The very steep and fine slopes (brown in Fig. 12) are areas of frequent occurrence of landslides and slope failures. A lack

111

of those types of slopes on the seafloor suggests the non-existence of rainfall erosion.

Fig. 13 shows a cut image of the terrain classification of a surrounding of the Seto Inland Sea by the clustering using the 150-m DEM. The whole area image can be found in Appendix-2. As for Fig. 12, deeper seafloor topography differs from the land in slope sizes. However, the Seto Inland Sea, which was formerly land before the last glacial period (Ota et al., 2004), shows unevenness like the land topography. The slopes shown in green or blue are distributed in alluvial plains, and the blue areas coincide with soft ground on the land. On the land, the yellow areas mainly correspond with sandy deposits such as fans, and the orange areas are slightly eroded slopes like terraces. The geological settings of the Seto Inland Sea (Yashima, 1994) seems to not contradict our classification.
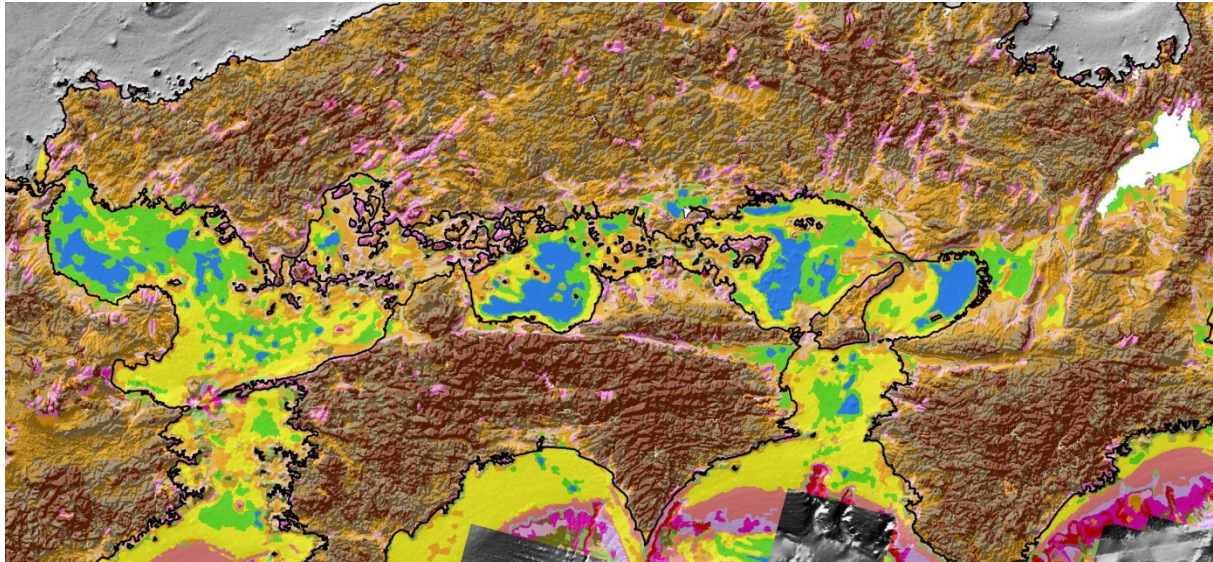

Fig. 13 Terrain classification of the Seto Inland Sea and its surroundings using the 150-m DEM. This map was created by object-based image segmentation using the three geometric signatures and classified by K-means clustering into 20 classes. The whole image from Kanto to Kyushu can be found in Appendix-2.

5. Cross-sections of the 3-D images of underground structure with the sea-land shaded-relief map

We planned to visualize the underground structure data with terrain surface data to help to understand the structure of Southwest Japan. We focused on the seismic tomography data (Matsubara and Obara, 2011) as the underground data. The data depth reaches hundreds of meters in depth and includes both land and sea areas, which cover the whole Southwest Japan and its surrounding seas. In this study, we edited the data by ArcGIS (ESRI) and visualization was done by Voxler (Golden Software).

Fig. 14 shows some slices above 200-km depth. More slices and the view of the high and low dVp sections can be found in Appendix-3. The overlaid data in Fig. 14 are as follows: the shaded-relief data of the 490-m DEM (this study), the dVp data calculated from the seismic tomography data (Matsubara and Obara, 2011), epicenters of 2011 (Japan Meteorological Agency), and the plate boundary of the Philippine Plate which is a combined GIS data of Baba et al. (2002), Nakajima and Hasegawa (2007) and Hirose et al. (2008) by Fuyuki Hirose of the Meteorological Research Institute (http://www.mri-jma.go.jp/Dep/st/member /fhirose/ja/PlateData.html). The dVp was developed as an index which makes underground structures intelligible (Matsubara et al., 2005). The dVp demanded the gap from the standard value of each depth to exclude influence of the increase of the earthquake wave velocity by the depth. High dVp values are interpreted to indicate hard or cold materials and low dVp to indicate soft or hot materials.

In the case of the orthogonal slices of the Nankai Trough, we can observe uneven views under the island arc, and characteristic high-dVp

sections (blue in Fig. 14) under the capes. In the case of the parallel slices, the most intriguing view is the three large low-dVp sections (red in Fig. 14) which are in the Philippine Plate. They seem to lay parallel to the boundary of the Pacific Plate. Especially, a large low-dVp section which grows under Shikoku to Osaka Bay may have relation to the "Kinki Spot" in Sano and Nakajima (2008), where some hot springs along Osaka Bay include magma source materials. The low-dVp sections just under Fuji Volcano or the Akaishi Mountains can also be well observed in the slices.
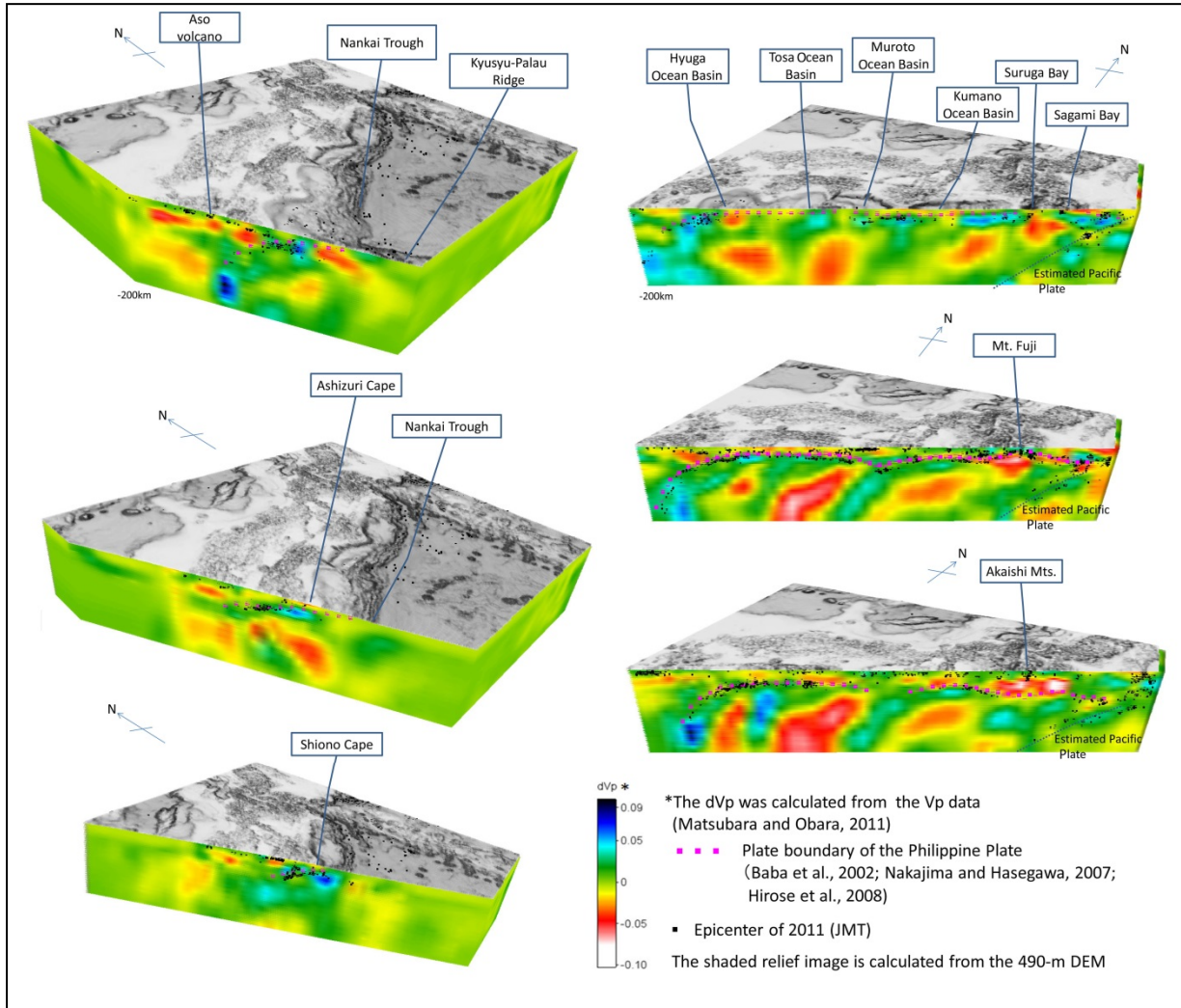

Fig. 14 The 3-D sliced views of the dVp data of Southwest Japan calculated from the seismic tomography (Matsubara and Obara, 2011) overlaid by the shaded-relief image of topography. More slices can be found in Appendix-3.

6.   Conclusions

The density and accuracy of elevation data has been improving for both the land and seafloor. In addition, GIS software and 3-D software on the market are also improved; therefore, it became easy to merge the elevation data of the land and seafloor, to analyze the topography, and to display it.

Drainage networks calculated from the 490-m sea-land combined DEM indicate that the places where drainage lines gather coincide with the post-Pleistocene turbidite deposits. We could find the watersheds of five large rivers continue to the Nankai Trough, though watersheds which fall to the Kumano ocean basin or the Hyuga ocean basin were not found.

The sea-land combined terrain classification using the 490-m DEM and the 150-m DEM shows the different view of the mountainous slopes on the land and the seafloor deeper than continental shelf, i.e., lack of fine texture slopes on the deep seafloor. In contrast, on shallow seafloor on the shelf, the Set

Inland Sea shows a similar view to the land.

We could observe a 3-D model of the seismic tomography intelligibly by adding the shaded-relief image of terrain surface and cutting the 3-D model into planes which are orthogonal or parallel to the Nankai Trough.

When observing a phenomenon which extends to the land and the sea, it is important to observe not only the surface of the land, but also the seafloor and the underground structures.

Acknowledgements

References

Asada, A. (2000): 500m mesh bathymetry data around Japan and visual edit program, Journal of Japan Society of Marine Survey Technology, Vol. 12, No. 1, pp.21-33. (in Japanese with English abstract and figures)

Baatz, M. and Schäpe, A. (2000): Multiresolution segmentation: an oprimization approach for high quality multi-scale image segmentation, In: Strobl, J., Blaschke, T., Griesebner, G. (Eds.), Angewandte Geographische Informations-Verarbeitung XII. Wichmann Verlag, Karlsruhe, pp. 12 – 23.

Baba, T., Tanioka, Y., Cummins, P. R. and Uhira, K. (2002): The slip distribution of the 1946 Nankai earthquake estimated from tsunami inversion using a new plate model, Physics of the Earth and Planetary Interiors, 132, pp. 59-73.

Blaschke, T. (2010): Object based image analysis for remote sensing, Vol. 65, issue 1, pp. 2-16.

Geographical Survey of Japan eds. (2014): Seamless digital geological map of Japan 1:200,000, Jan 14, 2014 version.

Gorvini, M.A.V. (2009): Physiographic classification of the ocean floor: a multi-scale geomorphometric approach, Proceedings of Geomorphometry 2009, Zurich, Switzerland, 31 August - 2 September, 2009.

Hay, G.J., Castilla, G., Wulder, M.A., and Ruiz, J.R. (2005): An automated object-base approach for the multiscale image segmentation of forest scenes. International Journal of Applied Earth Observation and Geoinformation, 7, pp. 339-359.

Hirose, F., Nakajima, J. and Hasegawa, A. (2008): Three-dimensional seismic velocity structure and configuration of the Philippine Sea slab in southwestern Japan estimated by double-difference tomography, Journal of Geophysical Research., 113, B09315, doi:10.1029/2007JB005274.

Hough, S.E., Altidor, J.R., Anglade D., Given, D., Janvier, M.G., Maharrey, J.Z., Meremonte, M., Mildor, B.S., Prepetit, C. and Yong, A. (2010): Localized damage caused by topographic amplification during the 2010 M7.0 Haiti earthquake, Nature Geoscience, 3, pp. 778-782.

Iwahashi, J. (1994): Development of landform classification using digital elevation model, Annuals of Disaster Prevention Research Institute of Kyoto University, No. 37, B-1, pp. 141-156. (in Japanese with English abstract and figures)

Iwahashi, J. and Kamiya, I. (1995): Landform classification using digital elevation model by the skills of image processing – mainly using the Digital National Land Information-, Geoinformatics, Vol. 6, No. 2, pp. 97-108. (in Japanese)

Iwahashi, J. and Pike, R. J. (2007): Automated classifications of topography from DEMs by an unsupervised nested-means algorithm and a three-part geometric signature. Geomorphology, 86, pp. 409-440.

Iwahashi, J. Kamiya, I. and Yamagishi, H. (2009): Estimation of the most suitable window size of the slope gradient and convexo-concave index for the

assessment of shallow landslides using high-resolution LiDAR DEM, Transactions, Japanese Geomorphological Union, Vol. 30, No. 1, pp. 15-27. (in Japanese with English abstract and figures)

Japan Association for Quaternary Research (1987): Explanatory Text for Quaternary Maps of Japan, University of Tokyo Press, 119pp., 4 sheets.

Kaizuka, S., Koike, K., Endo, K., Yamazaki, H., Suzuki, T. eds. (2000): Regional Geomorphology of the Japanese Islands: vol. 4 Geomorphology of Kanto and Izu-Ogasawara, University of Tokyo Press, 349pp. (in Japanese)

Machida, H., Ota, Y., Kawana, T., Moriwaki, H., Nagaoka, S. eds. (2001): Regional Geomorphology of the Japanese Islands: vol. 7 Geomorphology of Kyushu and the Ryukyus, University of Tokyo Press, 355pp. (in Japanese)

Machida, H., Matsuda, T., Umitsu, M., Koizumi, T. eds. (2006): Regional Geomorphology of the Japanese Islands: vol. 5 Geomorphology of Chubu Region, University of Tokyo Press, 385pp. (in Japanese)

MacQeen, J. (1967): Some methods for classification and analysis of multivariate observations, Berkley Symposium on Mathematical Statistics and Probability, Vol. 1, pp.281-297.

Maidment, D.R. eds. (2002): Arc Hydro: GIS for Water Resources, ESRI press, USA, 203pp.

Matsubara, M., Hayashi, H., Obara, K., and Kasahara, K. (2005): Low-velocity oceanic crust at the top of the Philippine Sea and Pacific plates beneath the Kanto region, central Japan, imaged by seismic tomography, Journal of Geophysical Research, Vol. 110, Issue B12, doi:10.1029/2005JB003673.

Matsubara, M. and Obara, K. (2011): The 2011 Off the Pacific Coast of Tohoku earthquake related to a strong velocity gradient with the Pacific plate, Earth Planets Space, 63, pp. 663-667.

Nakajima, J., and Hasegawa, A. (2007): Subduction of the Philippine Sea plate beneath southwestern Japan: Slab geometry and its relationship to arc magmatism, Journal of Geophysical Research, 112, B08306, doi:10.1029/2006JB004770.

Okuda, Y., Inoue, E., Ishibashi, K., Ishihara T., Kinoshita Y., Joshima M., Tamaki, K. (1977): Geologiccal Map off Outer Zone of Southwest Japan 1:1,000,000, Marine Geology Map Series, Geological Survey of Japan. (1 sheet)

Ota, Y., Naruse, T., Tanaka, S., Okada, A., eds. (2004): Regional Geomorphology of the Japanese Islands: vol. 6 Geomorphology of Kinki, Chugoku and Shikoku, University of Tokyo Press, 383pp. (in Japanese)

Reuter, H.I., Lado, L.R., Hengl, T. and Montanarella, L. (2008): Continental-scale digital soil mapping using European Soil Profile Data: Soil pH, Hamburger Beiträge zur Physischen Geographie und Landschaftsökologie, Heft 19, pp. 91-102.

Sano, Y. and Nakajima, J. (2008): Geographical distribution of ^{3}He/^{4}He ratios and seismic tomography in Japan, Geochemical Journal, Vol. 42, pp. 51 to 60.

Tarboton, D.G. (1998): A new method for the determination of flow directions and upslope areas in grid digital elevation models, Water Resources Research, Vol. 33, No. 2, pp. 309-319.

Tsutsumi, H., Nakata, H., Ogawa, M., Okamura, M., and Shimazaki, K. (1990): A preliminary report on the submarine Median Tectonic Line beneath northeastern part of Iyo-nada Sea, Southwest Japan, Active Fault Research, 8, pp. 49-57. (in Japanese)

Yashima, K. (1994): A geomorphological study of the caldrons in the Seto Inland Sea, Report of Hydrographic Researches, No. 30, pp. 237-327. (in Japanese with English summary)

Yong, A., Hough, S.E., Iwahashi, J., and Braverman, A. (2012): A terrain-based site-conditions map of California with implications for the contiguous United States, Bulletin of the Seismological Society of America, Vol. 102, No. 1, pp. 114-128.